Next-generation Cu(II) selective peptide shuttles prevent Cu(Aβ)-induced toxicity and microglial activation in organotypic hippocampal slices

Michael Okafor[1,2], David Schmitt[1,2], Stéphane Gasman[2], Laurent Raibaut[1], Christelle Hureau[4*], Peter Faller[1*#] and Nicolas Vitale[2*#]

[1] Laboratory of Biometals and Biological Chemistry, Institut de Chimie (UMR 7177), Université de Strasbourg-CNRS, 4 rue Blaise Pascal, 67000 Strasbourg, France

[2] Centre National de la Recherche Scientifique, Université de Strasbourg, Institut des Neurosciences Cellulaires et Intégratives, F-67000 Strasbourg, France

[3] Université de Strasbourg, CNRS, IPHC, UMR 7178, F-67000 Strasbourg, France

[4] LCC-CNRS, Université de Toulouse, CNRS, Toulouse, France

# Contributed equally to the work.

* corresponding authors : vitalen@unistra.fr, pfaller@unistra.fr, christelle.hureau@lcc-toulouse.fr, michael.okafor@icm-institute.org

Abstract

Alzheimer's disease (AD) remains the most prevalent neurodegenerative disease with hallmarks including the apparition, in specific areas of the brain, of intracellular neurofibrillary tangles and extracellular amyloid plaques. The latter result from an abnormal metabolism of Amyloid-β precursor protein (APP) leading to its accumulation in plaques. *Ex vivo* analysis of AD patients' brains, show an abnormally elevated concentration of metals including Cu, Zn and Fe in these plaques. Some studies have also demonstrated altered Cu levels in the entire brain and more specifically in regions heavily affected in AD. These modifications are often accompanied by a decline in neuronal Cu levels and by an increase in the proportion of extracellular labile Cu, which in turn promotes reactive oxygen species formation. To correct this Cu dyshomeostasis, we designed and synthesized novel Cu(II)-selective peptide shuttles, capable of swiftly retrieving Cu from extracellular Aβ and subsequently transporting and releasing Cu inside cells. We demonstrate here the capacity of this new Cu-shuttles, DapHH-αR5W4^{NBD} and HDapH-αR5W4^{NBD}, to protect organotypic hippocampal slices (OHSCs) from Cu(Aβ)-induced insult and their capability to rescues Cu-induced microglial activation and proliferation.

Key Words: Alzheimer disease, amyloid-b, copper, ROS, shuttle

Introduction

In Alzheimer's disease (AD), Copper (Cu) dyshomeostasis has been observed and is characterized by an extracellular accumulation of Cu in amyloid plaques, composed mainly of Aβ peptides, as well as a decrease in intracellular Cu levels in the brain[1,2] compared to healthy subjects. The Aβ peptides have been shown to be toxic, with most of their toxicity being exerted by intermediate-size species present during the self-assembly/aggregation of the peptides, also known as oligomers. Indeed, Aβ oligomers have been shown to induce cellular toxicity by directly forming pores in neuronal membranes, leading to their destabilization, as well as by disrupting the cytoskeleton, potentially leading to apoptosis[3]. Downstream, they have been shown to induce the formation of neurofibrillary tau tangles, which is strongly associated with AD stage progression and degenerescence [4–6].

Cu in its own regard is an essential metal for many living species and is therefore precisely regulated and dispersed within the organism to enable its participation in a large number of biological mechanisms. As Cu is essential for numerous cellular functions, a disturbance in its distribution can lead to a number of disorders including AD[7]. The loss of Cu homeostasis can lead to deregulation of normal Cuproprotein functions such as antioxidant defense, Iron (Fe) homeostasis or mitochondrial energy conversion[8]. Results from several groups have shown a general decrease in brain Cu levels in AD using various quantitative approaches[9,10]. In the same line, recent studies have shown a decrease in Cu levels in the cytoplasm of brain cells, which is associated with a 25% increase of exchangeable Cu in the brain (probably extracellular)[11,12]. Increase of Cu concentration in a biological compartment leads to the binding of Cu to unorthodox sites on proteins/ligands, potentially inducing a gain or loss of function. As such, the increment in the concentration of extracellular Cu labile pool leads to the binding of Cu on Aβ peptides [11–14]. Cu bound to Aβ can catalyze the formation of reactive oxygen species (ROS) aerobically in the presence of a reductant (e.g. ascorbate ($AscH^-$)) by cycling between Cu(I) and Cu(II) [15]. This reaction is possible because the Aβ peptide forms a complex with both Cu(II) (dissociation constant, $Kd \approx 10^{-9}$-10^{-10}) and Cu(I) ($Kd \approx 10^{-7}$-10^{-10}) at pH 7.4[16] and follows a very intricate mechanism[17]. It has therefore been proposed that Cu(Aβ) complexes contribute to the oxidative stress described in AD[18]. This stress takes various forms, ranging from peroxidation of cell membranes, oxidation of DNA and mitochondria[15,19]. Beyond their intrinsic toxicity, ROS can also participate to oxidatively modified $A\beta_{1\text{-}40/42}$ peptides leading to modified aggregation propensity or stronger resistance to endogenous degradation protease[20,21].

Cu thus seems to play an important role in AD progression. Therefore, restoring the homeostasis of this metal ion could reveal a critical goal unreached to date. This goal drove the design of metallophores that act as transmembrane transporters to shuttle metal ions, such as Clioquinol (iodochlorhydroxyquin, CQ) and its derivative, PBT2, as well as GTSM (glyoxal-bis(4-methylthiosemicarbazonato))[22–25]. These molecules are chelators of Cu(II) and Zn(II), forming neutral complexes capable of crossing the blood-brain barrier. They have shown convincing reduction in metal-modulated aggregation of Aβ peptides *in vitro*, accompanied by improved performances in various cognitive tests on AD murine models. CQ reached Phase II in clinical trial, showing improvement in various cognitive tests in advanced AD patients [26], but negative side-effects with prolonged treatment led to the end of the trial [27,28]. PBT2 was later developed as a safe CQ analog; however, it proved ineffective in phase II clinical trial [29]. Over the years, several additional small molecules have been developed to restore the correct Cu homeostasis lost in AD patients. Molecules such as GTSM and TDMQ20 have shown good results in AD models with preformed complexes [30,31]. These molecules have, however, a major pitfall as is seen for Elesclemol, a candidate for Menkes disease treatments[32]. Indeed they lack selectivity towards Cu(II), as they are known to bind Zn(II)[33].

We developed recently, a Cu(II)-selective peptide shuttle, AKH-αR5W4^{NBD}, capable of selectively retrieving Cu(II) from Aβ, stably binding Cu(II), thereby preventing Cu(Aβ)-induced ROS production. Once bound to Cu, AKH-αR5W4^{NBD}, is capable of importing bioavailable Cu into cells[34]. This shuttle is composed of three modular moieties: (1) an amino-terminal Cu(II) and Ni(II) binding motif (ATCUN), composed of the sequence Xxx1-Xxx2-His (with Xxx being any amino acid but proline) located on the N-terminal side, enabling selective binding of Cu(II) with high affinity ($Kd_{7.4} \approx 10^{-13}$-$10^{-15}$) [34] ; (2) a fluorophore, nitrobenzodiazole (NBD, with an excitation maximum at 480 nm and an emission maximum at 545 nm in aqueous medium) whose emission is quenched by the binging of Cu(II), allowing to monitor the Cu(II) binding and release; (3) a cell penetrating peptide (CPP), αR5W4, with sequence RRWWRRRWWR, for cell entry[35].

Preincubation of AKH-αR5W4^{NBD} for an hour in cellular media prior to the addition of $AscH^-$ and the subsequent triggering of Cu(Aβ) ROS formation was required for AKH-αR5W4^{NBD} to prevent Cu(Aβ)-induced toxicity on PC12 cells. In the present report, we describe two novel peptide shuttles that do not require pre-incubation to be effective. These molecules were inspired by recent work on ATCUN-based sequence with faster ability to bind Cu(II) or to retrieve it from Aβ [36,37]. Hence, a second His was introduced either in position 1 or 3. The two new sequences under focus here are based on Dap-His-His (DapHH) and His-Dap-His (HDapH), with Dap (2,3-diaminopropionic acid) being a shorter form of lysine. The non-conventional Dap amino-acid residues as well as its positioning inside the ATCUN sequence were chosen to permit a close proximity of NBD to the ATCUN binding sphere, thus we expect a total quenching of NBD fluorescence. The αR5W4 CPP was maintained and the ability of these shuttles (i) to retrieve Cu(II) from Aβ in complex biological media fast enough to stop Cu(Aβ)-induced ROS formation and (ii) to protect from Cu(Aβ)-induced toxicity was established in cellular and organotypic hippocampal slice culture models.

Materials and methods

Material

All compounds used during this study were purchased from accredited merchants including Dulbecco′s Modified Eagle′s Medium - high glucose (Sigma, D5796), MEM (Thermofisher, 12360038), Horse serum (Gibco, 26050070), Fetal calf serum (Gibco, 10270-160), Penicillin/streptomycin (Sigma, P4458), Trypsin (Gibco, 25300-054), MTT (Fisher Scientific, 10133722), Anti-Giantin antibodies (Abcam, ab24586), Monoclonal Anti-ATP7A antibodies (Abcam, ab13995), Recombinant Mouse Anti-Iba1 (Abcam, ab283319), Monoclonal Rabbit Anti-CD68 (Abcam, ab125212), Secondary antibodies (Life sciences) and Hoechst (Thermofisher, 62249).

Toxicity assay on PC12 cells

In 96 well plates, 50 000 cells were plated and incubated for 24h. A solution of monomerized Aβ complex in 10% DMEM (diluted with DMEM salt solution) was prepared in microcentrifuge tubes, followed with/without addition of AKH-αR5W4^{NBD}, DapHH-αR5W4^{NBD} or HDapH-αR5W4^{NBD} for 10 min or 1h. Afterwards, $AscH^-$ was added to the tubes and vortexed, the mixture was then added to PC12 cells. After 24h, the cell media was replaced with 200 µL of pure DMEM containing 10% of 5 mg/mL MTT solution and incubated for 4 h at 37°C. After a 4 h incubation at 37°C the medium was replaced with 150 µL DMSO and agitated for 5 min at room temperature. In a new 96 well plates, 50 µL solution of each well was diluted in 150 µL of pure DMSO solution. Lastly, the absorbance was read at 595 nm. Each condition corresponds to the average of three recordings on the same plate and each experiment was replicated independently three times.

ATP7A delocalization assay

Glass coverslips were treated with Poly-L-Lysine for 15 min in 4-well NUNC plates. Afterwards, the coverslips were rinsed with enriched DMEM media. PC12 cells were then cultured at a density of 1 x 10^5 per well, 24 h before experiments. In 10% DMEM solution, was added Cu shuttles alone or precomplexed to Cu(II). This mixture was added to the cells and incubated for 1 h. After the experiment, the medium was removed, and cells were fixed with 4% PFA (paraformaldehyde) then permeabilized and saturated in 0.2% Triton X-100 and 1X PBS containing 10% DS (Donkey serum) at 37°C. Cells were then incubated overnight at 4°C with chicken anti-mouse ATP7A 1/5000 and rabbit anti-mouse Giantin 1/500 in 3% BSA (Bovine Serum Albumin). The next day the cells were washed 3 times with PBS and then incubated with donkey anti-chicken, anti-rabbit secondary antibodies and Hoechst at 1/1000 dilution for 45 min at 37°C before being rinsed and mounted in Mowiol.

Organotypic hippocampal slice culture (OHSC)

The procedure recapitulates that of Stoppini et al. 1991 with minor modifications[38]. CD1 mice between ages P6 and P10 were used for OHSC. The dissection media consists of cold Hanks balanced salt solution (HBSS) and the llice culture media consists of 50% MEM solution, 25% HBSS, 25% Horse serum inactivated, 1% Strep-penicillin, 25 mM HEPES and 2 mM L-Glutamine. D-Glucose was added to the cell culture solution for a final concentration of 4.5 g/L (the Culture media should be at a pH 7.2).

Mice were decapitated and placed immediately in a 25 mL beaker containing ice cold HBSS. Using scissors, the skull was cut through and the brain extracted, then transferred to a 30 mm petri dish filled with cold HBSS. The hippocampus was extracted by holding down one hemisphere with forceps and separating the other with a spatula. Both hippocampi were extracted and placed on the Mcllwain tissue chopper board perpendicular to the blade, with the micrometer set at 400 µm and the blade wetted with cold HBSS before chopping. After brain slices were ready, the slices were transferred to a 30 mm petri dish filled with cold HBSS, and each slice was separated using 2 spatulas. Each slice containing the dentate gyrus, CA1, and CA3 regions, were placed on the Millicell insets with 6 hippocampal slices per well of a 6-well plate. The plate was placed in an incubator and the media was changed every 2-3 days. The slices were kept in culture for two weeks, to acclimatize to their new environment before experiment.

Cu toxicity rescue experiment OHSCs

After two weeks in culture, hippocampal slices were treated with different conditions for 48h in DMEM solution containing 25 mM HEPES. Prior to the experiment, preparation of Aβ monomers for monomeric conditions was carried out (see supplementary materials and methods).

Cu(II)Aβ complex was made by mixing 0.5 eq Cu (10 µM) with 1 eq Aβ (20 µM). After complexation of Cu(Aβ), DapHH-αR5W4^{NBD} or HDapH-αR5W4^{NBD} was added or not at 0.5 eq and vortexed. The solution was immediately placed on top of the slices (with time solution will drain into the well out of the Millicell inset). Slices were left for 48h at 37°C.

PI Staining*:* 100% DMEM salt containing 5 µM PI and 25 mM HEPES was prepared, and 100 µL was placed in each well on top of every slice and incubated for 1h at 37°C. Afterwards, slices were fixed with 4% PFA for 40 min. From each condition, 3 slices were cut out of the millicell insert after fixation and treated with Hoechst for 30 min and then mounted on slides. Slides were left at room temperature to semi-dry for 1 h and then images were acquired at 405 nm and 555 nm using a fluorescence microscope, ZEISS Axio Imager M2 coupled with a motorized board for mosaic imaging.

Immunohistochemistry*:* The remaining 3 slices were cut out of the millicell insert and were washed in PBS. The slices were permeabilized and nonspecific sites were blocked in PBS solution containing 0.3% triton and 10% Goat serum for 3 hours under agitation. Afterwards, slices were rinsed once in PBS and then incubated in PBS containing 1 mg/ml BSA (bovine serum albumin) overnight at 4°C with primary antibodies (Mouse Anti-Mouse Iba1 1:100 and Rabbit Anti-Mouse CD68 1:1000). Slices were washed 3 times in PBS for 5 min each with gentle shaking, and then incubated with secondary anti-mouse 555 nm and anti-rabbit 647 nm antibodies at 1:1000 dilution in PBS containing 1 mg/mL BSA for 3 hours at room temperature with gentle shaking. Finally, slices were washed 3 times in PBS for 5 min each with gentle shaking and mounted on glass slides by placing the slices with the membrane side flat on the slides. Mowiol was added on each slice followed by the cover. Slides were left to dry at room temperature in obscurity for at least 24h before confocal imaging using Leica SP5.

Analysis

Cell viability OHSC: Viability measurements were made by cell counting total cell number via the nucleus staining by Hoechst using the QuPath software. Cells were also incubated with propidium iodine (PI) and the mean fluorescence intensity of the PI staining was calculated in each cell nucleus. Cells with PI staining above a threshold were deemed PI positive and divided by the total cells (Hoechst positive) to give the percentage of Hoechst+ PI+ cells.

Microglia activation OHSC: Microglia activation analysis was carried out by labelling cells positive with both Iba1 and CD68. Iba1 cells were counted using QuPath software and labelled as microglia cells. From cells positive for Iba1, the average intensity of the microglial cells with a threshold of CD68 labelling were labelled as activated microglial cells. The percentage of activated microglial cells are expressed as CD68 positive cells divided by Iba1 positive cells. All data were normalized in respect to the control group.

Statistical analysis

All analyses were carried out using GraphPad prism 9.3.1. Data set underwent Shapiro test for normality. For comparisons of the mean, parametric test with Tukey Multiple Comparison post-test or non-parametric Kruskal–Wallis with Dunn's multiple comparisons test.

Fundings

This work was supported by a grant to N.V. from ITI Neurostra as part of the IdEx Unistra (ANR-10-IDEX-0002) under the framework of the French Program Investments for the Future. The IdEx PhD program, University of Strasbourg and the ITI Neurostra program (ANR-10-IDEX-0002) provided the salary to MO, and INSERM is providing the salary to NV and SG.

Acknowledgements

We acknowledge the Plateforme Imagerie In Vitro of ITI Neurostra at CNRS UAR-3256. Special thanks to Fréderic Doussau for his help with OHSC.

The authors declare that they have no conflicts of interest with the contents of this article.

Data availability

Data availability can be requested to the corresponding authors.

Results

Physico-chemical characterizations of Cu(II) peptide shuttles

First, potential differences in the physico-chemical properties of the new Cu(II)-selective peptides shuttles (DapHH-αR5W4^{NBD} and HDapH-αR5W4^{NBD}) in comparison to AKH-αR5W4^{NBD} were probed. The UV-Vis spectra display a similar absorption maximum at 490 nm and a small peak at 350 nm due to the NBD chromophore (Figure S1D). Thus, modifying the original ATCUN motif and the distance of the NBD fluorophore from the coordination sphere does not significantly impact the environment around the NBD fluorophore. However, an unexpected red-shift was observed for the complex formed between HDapH-αR5W4^{NBD} and Cu(II) (Figure S1E), indicating a structural change upon Cu(II)-binding.

The emission of both DapHH-αR5W4^{NBD} and HDapH-αR5W4^{NBD} were then studied by fluorimetry. The peptide shuttles were excited at 477 nm and the fluorescence spectra were recorded between 490 nm and 600 nm. An emission maximum was observed at 545 nm and the consequent addition of Cu(II) in a 0.1 equivalent step linearly decreased the emission intensity at 545 nm up to 1 equivalent (Figure S2A). For both DapHH-αR5W4^{NBD} and HDapH-αR5W4^{NBD}, 98% quenching of NBD emission was found, validating the intended design of the peptides (Figure S1A).

Next, we investigated the capacity of the shuttles to withdraw Cu(II) from cell culture media, DMEM 10% and DMEM/F12 1:1 (D/F). For this, we spiked DMEM 10% media or D/F media with 5 µM Cu(II) and incubated with AKH-αR5W4^{NBD}, DapHH-αR5W4^{NBD} or HDapH-αR5W4^{NBD} with NBD emission at 545 nm followed for 5h in a plate reader. Controls were carried out simultaneously in the absence of Cu and with the shuttles pre-complexed with Cu(II) before addition to the media, allowing to obtain the emissions at both the 100% saturated states and the 0% saturated states, respectively (Figure S3). DapHH-αR5W4^{NBD} or HDapH-αR5W4^{NBD} out-performed AKH-αR5W4^{NBD} in the rate of withdrawing Cu(II) from the cell culture media (Figure 1B and Table S1). All three peptide shuttles were capable of withdrawing Cu(II) from DMEM 10% media, however, only DapHH-αR5W4^{NBD} and HDapH-αR5W4^{NBD} were able to withdraw the majority of Cu(II) from D/F media over the 6h measurements (Figures 1B, S3 and Table S1), thereby confirming the successful design of shuttles with faster Cu(II)-binding ability. We then set out to validate the selectivity of DapHH-αR5W4^{NBD} or HDapH-αR5W4^{NBD} to withdraw specifically Cu(II) from cell media containing other essential d-block metal ions. For this, we spiked both DMEM 10% and D/F media with Cu(II), Fe(III), Zn(II) and Mn(II), each at 5 µM before addition of AKH-αR5W4^{NBD}, DapHH-αR5W4^{NBD} or HDapH-αR5W4^{NBD}. No major difference in the average kinetics or the withdrawal percentage of each of the three peptide shuttles in the presence or absence of other d-block metal ions was observed (Figures 1B, S4 and Table S1). However, HDapH-αR5W4^{NBD} seemed to be generally the fastest followed by DapHH-αR5W4^{NBD} and then AKH-αR5W4^{NBD}.

We next compared the kinetics of the selective withdrawal of Cu(II) by DapHH-αR5W4^{NBD} and HDapH-αR5W4^{NBD} to that of GTSM which is a known ionophore, capable of fast-binding Cu(II). Cu(II)GTSM complex has a characteristic charge transfer band at 477 nm with a molar extinction coefficient at 8 700 $M^{-1}cm^{-1}$ [39]. Using a UV-Vis spectrometer, we were able to follow GTSM selective retrieval of Cu(II) from DMEM 10% and D/F media (Figure S5). GTSM displayed comparable kinetics of Cu(II) withdrawal in comparison to that of HDapH-αR5W4^{NBD} in both DMEM 10% and D/F media (half-time <1 min).

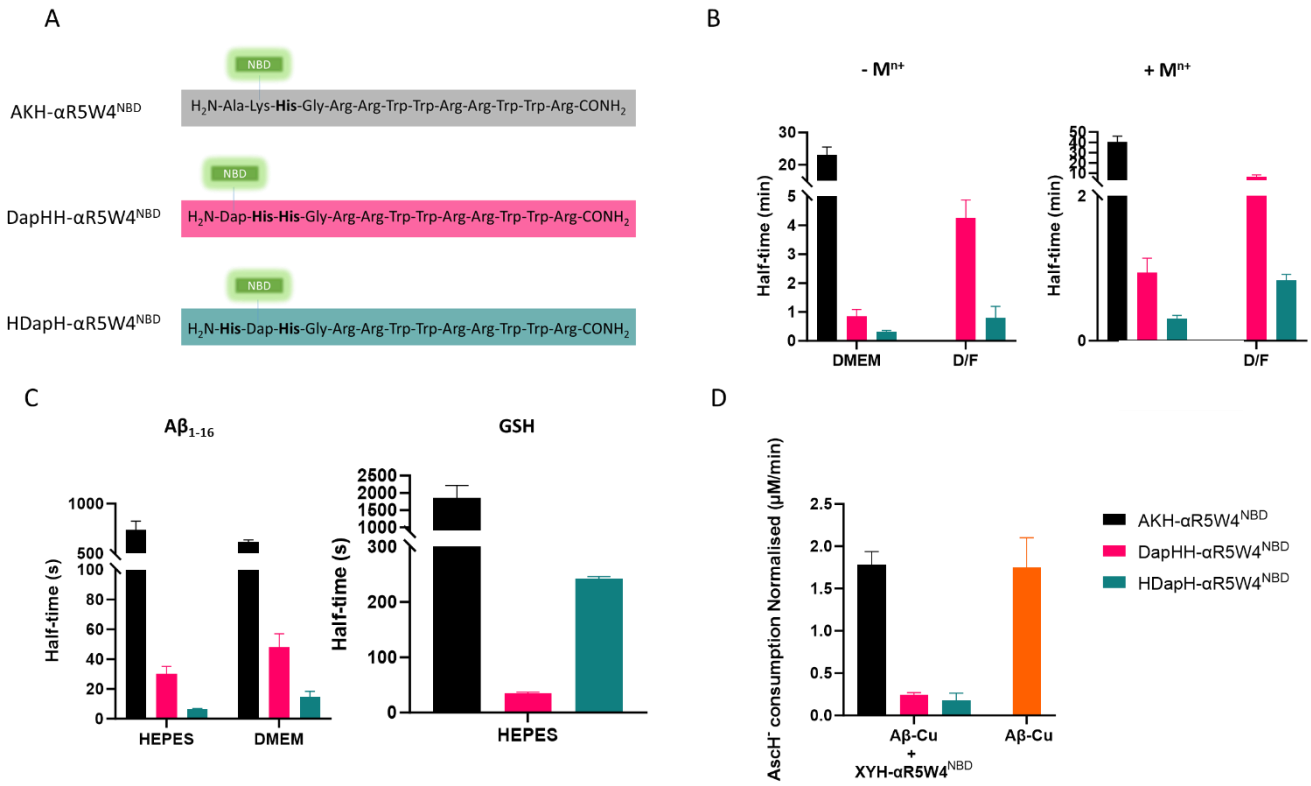

Figure 1: The novel Cu(II)-selective shuttles have a faster Cu(II) binding kinetic. (**A**) Amino acid sequence of XYH-αR5W4^{NBD} (AKH-αR5W4^{NBD}, DapHH-αR5W4^{NBD} or HDapH-αR5W4^{NBD}). (**B**) Half-time of the selective withdrawal of Cu(II) by XYH-αR5W4^{NBD} in cell culture media containing Cu(II) alone or in addition to M^{n+} (Fe (III), Zn(II) and Mn(II)). Of note, AKH-αR5W4^{NBD} Cu(II) withdrawal was too slow in D/F media, data not shown. Conditions: Cu(II)=AKH-αR5W4^{NBD}=DapHH-αR5W4^{NBD}=HDapH-αR5W4^{NBD}= 5 µM, DMEM 10%, D/F 100%, 25°C, n=3. **(C)** Retrieval of Cu(II) from Aβ$_{1-16}$ by XYH-αR5W4^{NBD}, in HEPES or DMEM 10% media and reduction/release of Cu(II) bound to XYH-αR5W4^{NBD} by GSH in HEPES. Conditions: AKH-αR5W4^{NBD} =DapHH-αR5W4^{NBD}=HDapH-αR5W4^{NBD}= 5 µM; Aβ$_{1-16}$ =10 µM; Cu(II)=5 µM, HEPES 100 mM pH 7.4, 25°C, n=3. **(D)** Inhibition of AscH$^-$ consumption by XYH-αR5W4^{NBD} monitored by the absorbance of AscH$^-$ at 265 nm see Figure S2E. Addition of AscH$^-$ was carried out at t_0 and Cu(II)Aß$_{1-16}$ at t_5 and addition of XYH-αR5W4^{NBD} at t_{10}. Graph shows the initial consumption of ascorbate in the first 20 min after addition of shuttles in the presence of Cu(II)Aß$_{1-16}$, normalised with values from samples in the absence of Cu(II)Aß$_{1-16}$. Conditions: AscH$^-$= 100 µM, Cu(II)DapHH-αR5W4^{NBD}=Cu(II)HDapH-αR5W4^{NBD}= 5 µM, Aß$_{1-16}$= 10 µM, Cu(II)= 5 µM, HEPES 100 mM pH 7,4. n=2 independent experiments. Of note Data for AKH-αR5W4^{NBD} (Figure1C,D) has been already published[34].

Given the faster kinetics gained by the novel peptide shuttles in withdrawing Cu(II) from cell culture media, we investigated their capacity to withdraw Cu(II) from Aβ$_{1-16}$, the domain responsible for Cu binding in Aβ peptides [20,40]. Very fast retrieval of Cu(II) from Aβ$_{1-16}$ was observed in either HEPES solution or 10% DMEM (Figure S2B,C) for both peptides, with HDapH-αR5W4^{NBD} being the fastest (**Error! Reference source not found.**Figure 1C). More precisely, the shuttles DapHH-αR5W4^{NBD} and HDapH-αR5W4^{NBD} retrieved Cu(II) completely from Aβ$_{1-16}$ in less than 2 min, compared to about 1 hour for AKH-αR5W4^{NBD} shuttle. We then investigated the capacity of physiological levels of GSH to reduce Cu(II) on either DapHH-αR5W4^{NBD} or HDapH-αR5W4^{NBD}. Reduction of Cu(II) by a cellular reducing agent like GSH renders the Cu bioavailable. Results show that both DapHH-αR5W4^{NBD} and HDapH-αR5W4^{NBD} have half-times of a few minutes while that of AKH-αR5W4^{NBD} peptide was tens of minutes. Intriguingly, DapHH-αR5W4^{NBD}

has a faster Cu(II) reduction rate than HDapH-αR5W4^{NBD} (Figure 1C and Figure S2D). We then tested the capacity of the Cu-shuttles to inhibit Cu(Aβ)-induced ROS production catalysed by AscH$^-$ by monitoring AscH$^-$ at 265 nm. The initial rate of ROS production by Cu(II)Aβ$_{1-16}$ measured during the first 20 minutes after addition of AscH$^-$ is 1.6 ± 0.1 µM/min. Upon addition of DapHH-αR5W4^{NBD} or HDapH-αR5W4^{NBD}, an immediate slow-down in ROS production was observed (Figure 1D and S1E), which was not the case for AKH-αR5W4^{NBD} shuttle without preincubation[34].

In summary, both DapHH-αR5W4^{NBD} and HDapH-αR5W4^{NBD} have proven to be kinetically much faster than AKH-αR5W4^{NBD}, in retrieving Cu(II) from Aβ$_{1-16}$ and therefore in stopping Cu(Aβ)-induced ROS production. In brief, the changes made in the shuttle sequences have proven to be effective with a fast enough Cu(II) removal out of Aβ to stop Cu(Aβ)-induced ROS production without the need for preincubation. In the next studies, we will show that in addition, these new shuttles are able to transfer and release Cu intra-cellularly while preventing cells from extracellularly Cu(Aβ)-induced ROS toxicity.

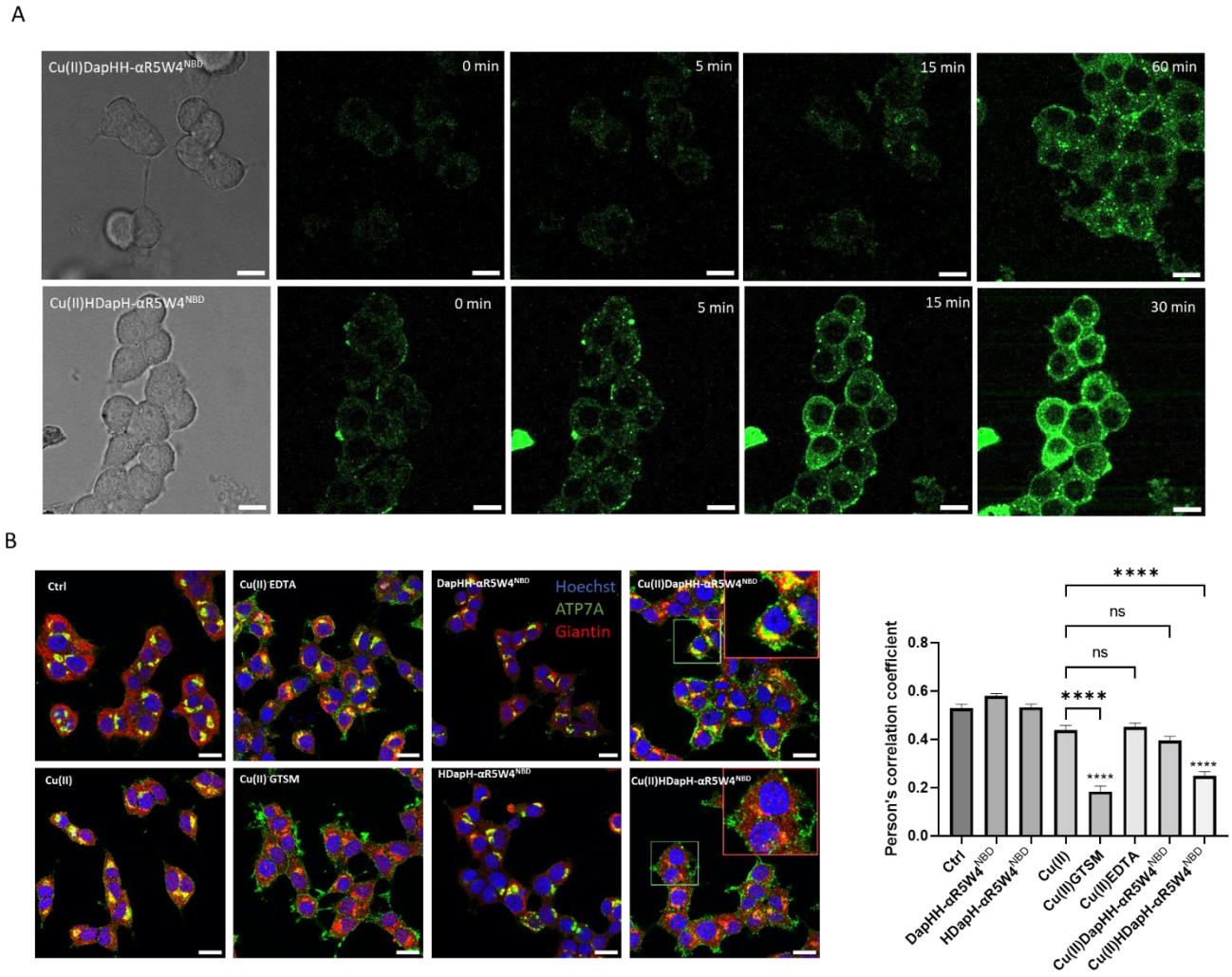

Figure 2: Cu import by XYH-αR5W4^{NBD} induced delocalization of ATP7A from the TGN to vesicular structures. (A) Representative images at the indicated time obtained from live imaging performed on 5 x 10 ^{4} PC12 cells incubated with 5 µM Cu(II)DapHH-αR5W4^{NBD} or Cu(II)HDapH-αR5W4^{NBD}, at 37°C using a Leica TCS SP5 (II) confocal microscope, with an excitation wavelength at 477 nm for 30 min. Time point zero is about 1 minute after

incubation with the peptide shuttles. Bars = 10 µm. Similar observations were obtained with 5 different cell cultures. **(B)** Quantification of the colocalization between ATP7A and Giantin staining was measured as the Pearson's correlation coefficient. PC12 cells were incubated for 1h in DMEM media alone (control = Ctrl) or, 5 µM Cu(II), Cu(II)-EDTA, DapHH-αR5W4^{NBD}, Cu(II)DapHH-αR5W4^{NBD}, Cu(II)HDapH-αR5W4^{NBD}, HDapH-αR5W4^{NBD} or 1 µM Cu(II)-GTSM, before fixation and processed for immunostaining; Blue: Hoechst (Nucleus marker); Green: ATP7A; Red: Giantin (Golgi marker). Representative images are shown. Bars = 10 µm. n=3 independent experiments. A zoomed inset is displayed on Cu(II)-DapHH-αR5W4^{NBD} and Cu(II)-HDapH-αR5W4^{NBD} .Number of cells analyzed ≥ 27 for each condition. A parametric ordinary one-way ANOVA test was carried out with a Dunnett's Multiple Comparison Test **** p<0,00001.

Cellular characterization of DapHH-αR5W4^{NBD} and HDapH-αR5W4^{NBD} in PC12 cells

Having characterized the Cu(II) coordination properties of DapHH-αR5W4^{NBD} and HDapH-αR5W4^{NBD}, we next tested their properties on PC12 cells, a well-known neurosecretory cell model. Neither DapHH-αR5W4^{NBD} or HDapH-αR5W4^{NBD} nor the corresponding Cu(II) complexes were toxic until above 10 µM (Figure S6A). This points to the fact that micromolar concentration of the peptide shuttles unlike GTSM (Figure S6B) do not lead to intracellular toxic levels of Cu.

We then investigated cell entry of these peptides into PC12 cells using confocal microscopy. Over a 30 min incubation, we observed a gradual increase in intracellular fluorescence attributed to an increased intracellular penetration of peptide shuttles (Figure S7). The fluorescence signal mostly corresponded to intracellular vesicles similar to endosomes, which points to a cell entry mechanism involving endocytosis as recently established for the αR5W4 CPP[35]. Interestingly, upon treatment of PC12 cells with 5µM Cu(II)(DapHH-αR5W4^{NBD}) or Cu(II)(HDapH-αR5W4^{NBD}), lower levels of fluorescence was seen within the first minutes of incubation which may be explained by Cu(II) quenching of NBD fluorescence mirroring that the complex was still intact early after cellular entry (Figure 2 and Figure S7). With time, there is more fluorescence in intracellular vesicles for Cu(II)(HDapH-αR5W4^{NBD}), however, Cu(II)(DapHH-αR5W4^{NBD}) only has an increase in fluorescence after an hour of incubation. This points to the possibility of Cu release by our shuttles through another mechanism than the reducing environment of endosomes.

Having validated that Cu(DapHH-αR5W4^{NBD}) and Cu(HDapH-αR5W4^{NBD}) i) can penetrate into PC12 cells and ii) are located inside vesicular structures, iii) may gradually release Cu within endosomes, we then looked at the bioavailability of the imported Cu, indirectly, through the delocalisation of the Golgi-associated Cu transporter, ATP7A. This protein is known to delocalise from the perinuclear Golgi area to vesicles in proximity to the plasma membrane, when the cell needs to expel Cu in excess[41]. Treatment with Cu(II)HDapH-αR5W4^{NBD} induced a significant delocalisation of ATP7A on vesicular structures close to the plasma membrane in PC12 cells after 1h incubation, thereby confirming the presence of cytosolic bioavailable Cu (Figure 2B). This is, however, not the case for Cu(II)DapHH-αR5W4^{NBD} , which is in line with a lower signal of DapHH-αR5W4^{NBD} in cells (Figure 2A) and most likely suggesting a slower release of cellular bioavailable Cu by this shuttle.

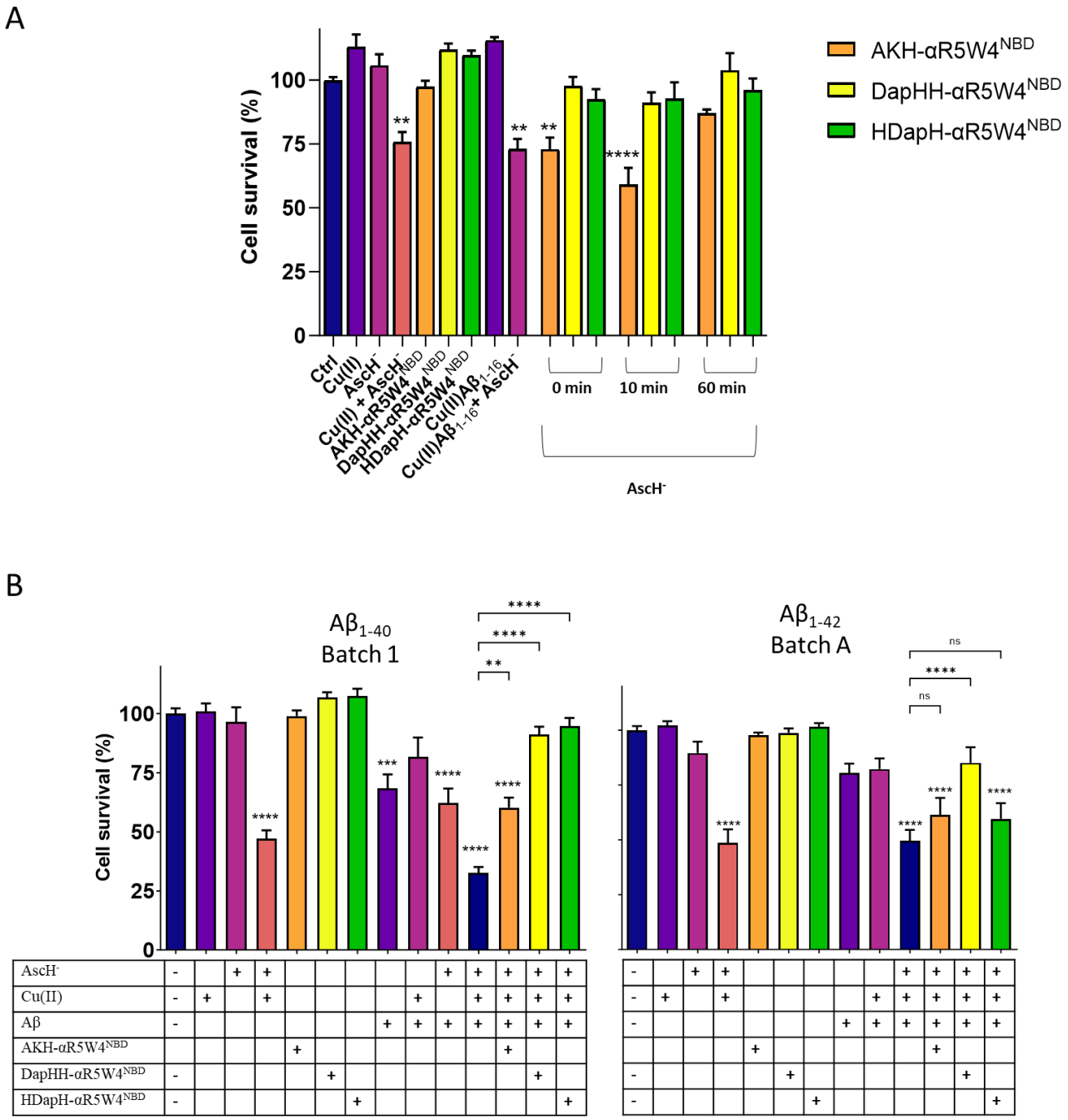

Figure 3: Transfer of Cu(II) from Aß to ATCUN motif prevents Cu-induced ROS production and toxicity to PC12 cells. (**A**) 5 µM AKH-αR5W4^{NBD}, DapHH-αR5W4^{NBD} or HDapH-αR5W4^{NBD} were pre-incubated with 10 µM Cu(II)Aβ_{1-16} 0.5:1 in 10% DMEM in a test tube for 0, 10 or 60 min before addition of 500 µM AscH$^-$ and immediate administration on the PC12 cells. Experiments were done in triplicates, n=3. Passed a normality D'Agostino & Pearson test. A parametric ordinary one-way ANOVA test was carried out with a Tukey Post Test * p<0,01, ** p<0,001, **** p<0,00001. (**B**) PC12 cells were incubated with 5 µM AKH-αR5W4^{NBD}, DapHH-αR5W4^{NBD} or HDapH-αR5W4^{NBD} with 10 µM Cu(II)Aβ_{1-40} 0.5:1 and 500 µM AscH$^-$ for 24h. Experiments were done in triplicates, n=3. A parametric ordinary one-way ANOVA test was carried out with a Tukey's multiple comparison Test * p<0,01, ** p<0,001, **** p<0,00001. Experiments were carried out in 10% DMEM.

Next, we investigated the ability of DapHH-αR5W4^{NBD} and HDapH-αR5W4^{NBD} to protect PC12 from Cu(II) A$\beta_{1-16/40/42}$-induced toxicity in the presence of AscH$^-$. Cu(II)Aβ_{1-16} was toxic only in the presence of the reductant AscH$^-$. This toxicity was reversed in the presence of DapHH-αR5W4^{NBD} or HDapH-αR5W4^{NBD}, but not in the presence of AKH-αR5W4^{NBD} which required pre-incubation to prevent toxicity (Figure 3A**Figure**). This is in line with the faster retrieval of Cu(II) from Aβ and arrest of ROS production by the novel shuttles as previously demonstrated *in vitro* (Figure 1). Indeed, AKH-αR5W4^{NBD} was able to significantly rescue Cu-induced toxicity after 1h pre-incubation as reported previously[34].

The rescue of PC12 cells from Cu-induced toxicity was studied using independent batches of Aβ_{1-40} peptides. In agreement with the known variability in Aβ-induced cell toxicity[42], of the three batches tested, only batch 1 and 2 had a significant toxicity on PC12 cells at 10 µM with batch 3 showing only a tendency (Figure 3B, Figure S8). In the presence of Cu(II)-Aβ_{1-40}, upon addition of AscH$^-$, there was a significant increase in toxicity for all three Aβ_{1-40} batches as a result of ROS production, as observed for Aβ_{1-16} (Figure 3A). DapHH-αR5W4^{NBD} and HDapH-αR5W4^{NBD} rapidly and fully rescued this toxicity due to Cu(II)Aβ_{1-40} in the presence of AscH$^-$ without need for pre-incubation. DapHH-αR5W4^{NBD} was equally fully protective in the presence of Cu(II)Aβ_{1-42} and AscH$^-$ whereas like AKH-αR5W4^{NBD}, HDapH-αR5W4^{NBD} only partially preserved cell survival (Figure 3B). In conclusion, the novel Cu(II)-selective peptide shuttles, DapHH-αR5W4^{NBD} or HDapH-αR5W4^{NBD}, are capable of instantly preventing Cu(II)Aβ_{1-16} and Cu(II)Aβ_{1-40} induced toxicity on PC12 cells in the presence of AscH$^-$, whereas only DapHH-αR5W4^{NBD} was able to instantly rescue Cu(II)Aβ_{1-42} toxicity.

Organotypic hippocampal slice culture (OHSC) model of AD

We next evaluated the protective properties of these peptide shuttles in a more complex model using organotypic hippocampal slice culture (OHSC) with visible dendate gyrus (DG), CA3, CA2, and CA1 obtained from CD1 mice between P6-P10 and placed in culture for 2 weeks before treatment. Hippocampal slices were incubated with Cu(II)Aβ_{1-40} or Cu(II)Aβ_{1-42} with or without the presence of DapHH-αR5W4^{NBD} and HDapH-αR5W4^{NBD} for 48h without supplementation with AscH$^-$ because the brain intrinsically possesses between 0.1 – 1 mM AscH$^-$[43,44], in contrast to cultured 2D cells[45].

Cell density analysed by counting the number of nuclei, labelled by Hoechst was similar for each condition validating slice quality and absence of variability (Figure 4). Cell toxicity on organotypic hippocampal slices was determined by treating slices for 1h with propidium iodide (PI) before staining with Hoechst as PI-labelled cells, represent cells that have a compromised plasma membrane thus permitting the nuclei intercalate PI to bind to cell DNA. Of note, PI staining does not directly detect cell death, but rather permeabilization of the plasma membrane.

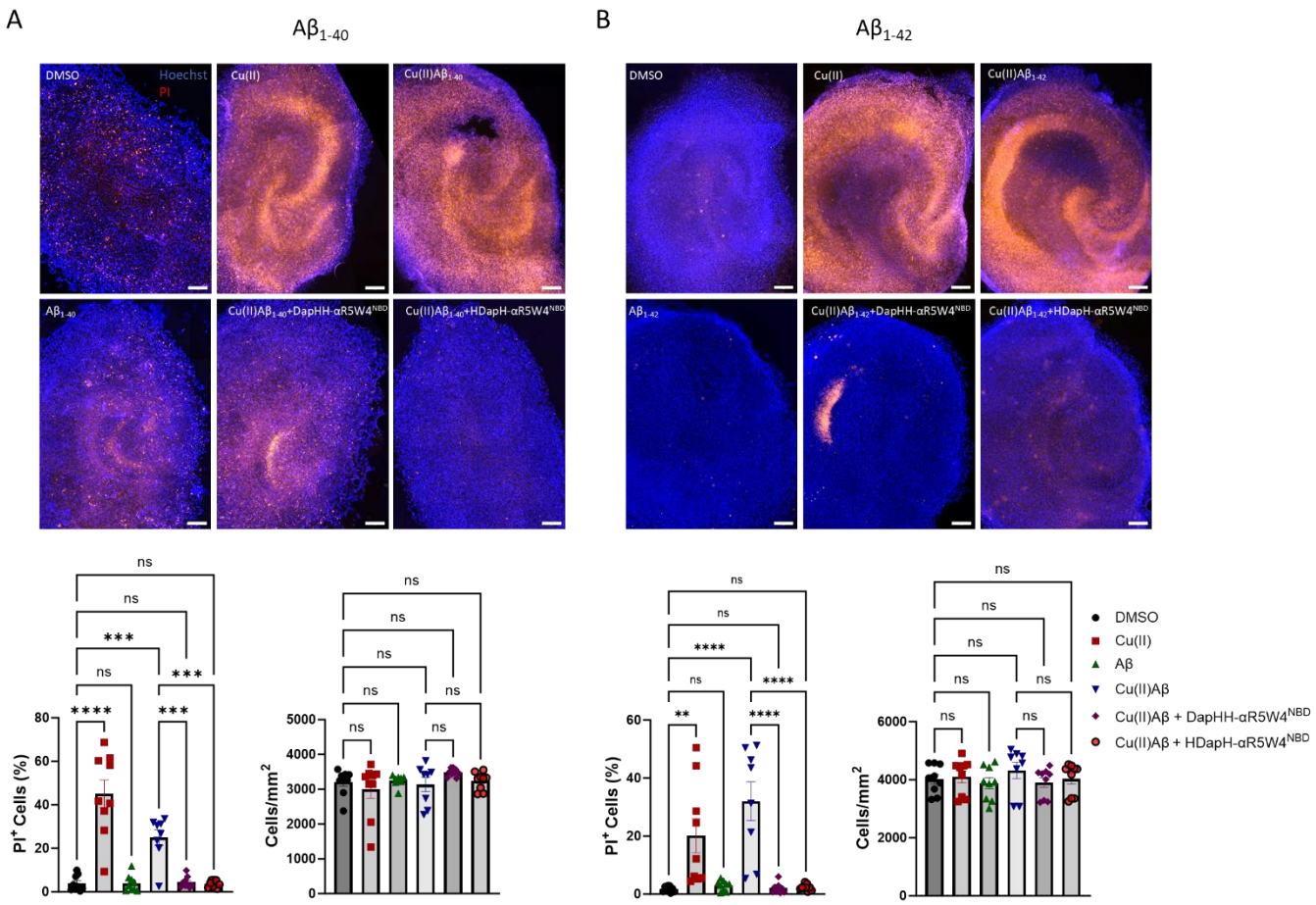

Figure 4: Novel Cu(II)-selective peptide shuttles rescue Cu(II) induced cell toxicity in OHSC. (A) Effect of Cu(II)Aβ_{40} or **(B)** Cu(II)Aβ_{42} on OHSC toxicity. Representative images of the effect of Cu(II) peptide shuttles on Cu-induced Cu(II)A$\beta_{40/42}$ toxicity on OHSC with analysis of the preventive effect of DapHH-αR5W4^{NBD} or HDapH-αR5W4^{NBD} on Cu(II)A$\beta_{40/42}$ induced toxicity and analysis of the cell density in OHSCs culture after 48h treatment. Conditions: Cu(II)=DapHH-αR5W4^{NBD}=HDapH-αR5W4^{NBD}=10 µM, Aβ_{40}=Aβ_{42}= 20 µM. Hoechst is blue, with PI being red. A non-parametric test was carried out with a Kruskal-Wallis Multiple Comparison Test for Cells/mm^2 for both Aβ_{40} and Aβ_{42}. A parametric ordinary one-way ANOVA test was carried out with a Tukey's Multiple Comparison Test for PI$^+$ cells for both Aβ_{40} and Aβ_{42},** p<0,001, *** p<0,0001, **** p<0,00001. n=3 independent experiments with at least 3 slices per condition.

Treatment of organotypic hippocampal slices with 20 µM of monomeric Aβ_{1-40} or Aβ_{1-42} for 48h did not lead to detectable toxicity (Figure 4). We thus adapted a protocol for aggregation of Aβ_{1-42} which was also unable to induce any toxicity (Figure S9), in disagreement with previous observations[46,47]. This may result from poor aggregation of this Aβ_{1-42} batch in these conditions.

In Cu(II) treated cells, there was a significant increase in PI-stained nuclei, which suggests that 10 µM of extracellular Cu(II) is toxic to organotypic hippocampal slices, in accordance with reports showing that sub-neurotoxic concentration of Cu(II) (10 µM) was able to activate microglia in primary cell culture, which may also trigger neuronal damage[48]. Alternative hypothesis for this Cu-induced toxicity include neuronal Cu overloading and ROS and microglial activation by Cu "loosely" bound to an extracellular ligand.

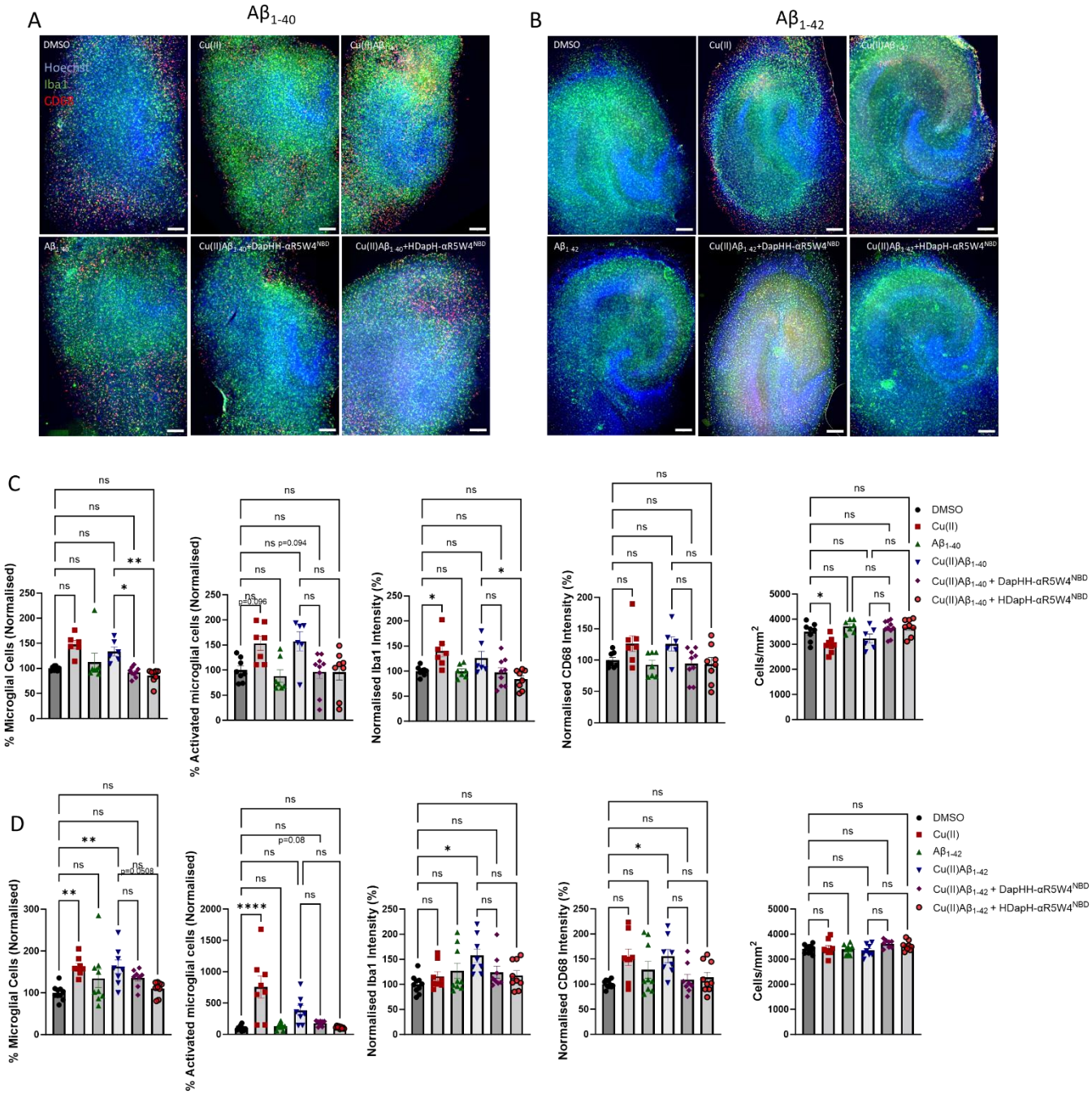

Figure 5: Effect of DapHH-αR5W4^{NBD} or HDapH-αR5W4^{NBD} on Cu(II)-induced microglia proliferation and activation. (A-B) Representative images of the effect of Cu(II) peptide shuttles on Cu-induced Cu(II)A$\beta_{40/42}$ microglia activation on OHSC with **(C-D)** analysis of the preventive effect of DapHH-αR5W4^{NBD} or HDapH-αR5W4^{NBD} on Cu(II)A$\beta_{40/42}$ induced microglia proliferation, activation, and analysis of the cell density in OHSCs culture after 48h treatment. Hoechst is blue, Iba1 green and CD68 being red. Conditions: Cu(II)=DapHH-αR5W4^{NBD}=HDapH-αR5W4^{NBD}=10 µM, Aβ_{40}=Aβ_{40}= 20 µM. A non-parametric test was carried out with a Kruskal-Wallis Multiple Comparison Test for activated microglial cells and % microglial cells for Aβ_{40} and normalized Iba1

intensity for $A\beta_{42}$. A parametric ordinary one-way ANOVA test was carried out with a Tukey's Multiple Comparison Test for the rest, * p<0,01,** p<0,001, *** p<0,0001, **** p<0,00001. n=3 independent experiments with at least 3 slices per condition.

Treatment with Cu(II)$A\beta_{1-40}$ or Cu(II)$A\beta_{1-42}$ also triggered an increase in slice toxicity, which could be attributed to Cu(II) toxicity (Figure 4, S9). In hippocampal slices co-incubated with Cu(II)$A\beta_{1-40/42}$ and DapHH-αR5W4^{NBD} or HDapH-αR5W4^{NBD}, there was a complete rescue in toxicity induced by Cu(II). Together, this set of results goes in the line with what has been observed previously in PC12 cells and also reinforce the hypothesis that the Cu(II)-induced toxicity can be attributed to an extracellular effect. In other words, the toxicity observed in our assays is probably not the consequence of an increase in intracellular Cu levels, which is expected to be further increased by the shuttles, but rather result from interaction with "free" or "loosely" bound Cu promoting ROS formation. Most importantly, these novel Cu shuttles were found to very effectively prevent this Cu(II)-$A\beta_{1-40/42}$ induced toxicity on OHSCs.

Given that Cu(II) could both directly or through ROS production induce microglia activation [48–50], treated slices were stained using Iba1, a pan microglia marker[51] and CD68, a marker of activated microglia[52]. Microglial cells were quantified by counting the cells positive for Iba1, and the percentage of microglial cells was calculated by considering total cells, represented by Hoechst staining. Treatment of organotypic hippocampal slices with Cu(II), Cu(II)$A\beta_{1-40}$ or Cu(II)$A\beta_{1-42}$ induced an increase in the percentage of microglial cells in regard to DMSO treated slices (Figure 5). Since there is no significant change in the density of cells in OHSCs after treatment with Cu(II)$A\beta_{1-40/42}$ (Figure 4), this could signify a combination of induced proliferation of microglial cells and death of other neural cells in Cu(II) treated OHSC slices. In slices, co-incubation with DapHH-αR5W4^{NBD} or HDapH-αR5W4^{NBD} reduced microglial cell proliferation induced by Cu(II)$A\beta_{1-40/42}$ (Figure 5). Equally, there was an increase in microglial activation in Cu(II), Cu(II)$A\beta_{1-40}$ or Cu(II)$A\beta_{1-42}$ treated slices, as seen by an increase in CD68 labelling in microglial cells (Iba1 and CD68 positive cells), which was efficiently prevented by co-incubating Cu(II)$A\beta_{1-40}$ or Cu(II)$A\beta_{1-42}$ treated slices with the Cu shuttles. Similar observations were found in slices treated with Cu(II)$A\beta_{1-42}$ after a protocol for $A\beta_{1-42}$ aggregation (Figure S9). In conclusion, the novel Cu(II)-selective shuttles DapHH-αR5W4^{NBD} and HDapH-αR5W4^{NBD} display protective activity towards brain tissue from Cu-induced insult.

Discussion

Over recent years, Cu has been studied for its role in many pathologies including Wilson disease, Menkes disease and several neurodegenerative diseases[53–64]. Although the origin of Cu dysfunction has been elucidated in some cases (Wilson disease and Menkes disease), there is still a lot of open questions as to the mechanisms leading to these Cu dyshomeostasis. There is also clearly more work needed to understand how the loss of Cu homeostasis affects different parts of the body such as the brain. In this context, tools to study Cu-metabolism on different levels from cell culture to *in vivo* models are crucial to better delineate the mechanisms. There are currently only few studies employing Cu(II)-selective fluorescence sensing probes capable of entry inside cells[65,66]. Although the molecules used in these studies penetrate cell membrane, they have either a very weak affinity for Cu(II) or are not specific for Cu(II). Here, we have synthesized novel Cu(II) sensitive ligands, termed Cu shuttles. These Cu shuttles have been characterized at the physico-chemical level and show high affinity for Cu(II) due to their ATCUN motif (Log $K_{7.4} \approx 10^{13\text{-}15}$). A novelty in our Cu(II) selective shuttles is their ability to import selectively Cu into cells and also to release Cu once inside the cells. Of note, other Cu shuttles, such as GTSM, Clioquinol, PBT2 or Elesclomol are generally less selective for Cu(II) in a biological setting[22,67,68]. Another advantage of our shuttles is their ability to be tracked in real time, once in the cell, since they are equipped with a fluorophore close to the Cu(II) coordination sphere, which permits up to 98% fluorescence quenching. Hence, dequenching of the shuttle upon Cu release inside the cells should provide both temporal and subcellular resolution as to the release of Cu. This makes the Cu shuttles, AKH-αR5W4^{NBD}, DapHH-αR5W4^{NBD} and HDapH-αR5W4^{NBD}, well-suited for mechanistic studies to follow Cu importation in cells.

The novel shuttles described here were successfully designed to have faster Cu(II)-binding kinetics compared to AKH-αR5W4^{NBD}. Indeed, our studies in cultured cells and hippocampal organotypic slices clearly showed the importance of this feature as the DapHH-αR5W4^{NBD} and HDapH-αR5W4^{NBD} were able to stop ROS production immediately and protect cells/tissue against Cu(II)-Aβ induced toxicity without any need for preincubation. This can be explained by the instantaneous stop of Cu(II)-Aβ-induced ROS production through the faster Cu(II) retrieval from Aβ combined with the shuttle entry into the cell with Cu.

The intracellular kinetics and mechanism of Cu release of the Cu shuttles is likely to be of importance, along with the intracellular location of Cu release. For instance, it is possible that the cell toxicity induced by GTSM results from too high levels, too fast release, and/or release of Cu in inappropriate intracellular compartments. Therefore, it is important for these novel Cu shuttles to release Cu in the cells where it is needed, for example the cytoplasm, and for these molecules not to induce cuprotoxicity. Indeed it is anticipated that a slow and gradual release of Cu(II) in vesicular structures might be beneficial and less toxic to the cell as compared to a fast intracellular accumulation of Cu. We first hypothesized that the Cu-release from the Cu-shuttle described here occurs through GSH reduction. Although *in vitro* data showed that reduction by GSH is possible (Figure 1C), *in cellulo* data indicated that reduction is probably not the major mechanism, given that AKH-αR5W4^{NBD} and HDapH-αR5W4^{NBD} releases Cu quicker into the cells than DapHH-αR5W4^{NBD} (Figure 2B), while the latter is the most sensitive to GSH. An alternative hypothesis is that the progressive lowering of pH occurring in the endolysosomal pathway, the major cellular entry routes used by αR5W4 CPP[35], might be the most important cause of Cu release from the shuttles. Indeed, the different Cu(II)-motifs in each shuttle do not respond to pH in the same way, in particular for the DapHH-αR5W4^{NBD}. The XHH motif of DapHH-αR5W4^{NBD} has two Cu(II) binding modes (3N and 4N). At neutral pH, there is an equilibrium of two binding modes, with 4N being the majority[36,37,69,70]. However, at low pH values, the 3N form is predominant. This means that DapHH-αR5W4^{NBD} could bind to Cu(II) at the later phases of endosomal acidification which might not be the case for HDapH-αR5W4^{NBD}. Hence, the release of Cu(II) from the Cu-shuttles could be triggered by lowering the pH in addition to or instead of Cu(II)

reduction. Supposing that the cellular entry mechanism of the different shuttles based on the αR5W4 CPP is similar, this suggests that the release of Cu(II) by AKH-αR5W4^{NBD} and HDapH-αR5W4^{NBD}, might occur early in the endolysosomal compartment as they can't withstand the acidity of these compartments, whereas the release of Cu(II) by DapHH-αR5W4^{NBD} would occur in the lysosome at lower pH.

Another factor to be considered when using Cu(II) ionophores is the toxicity that can arise from the import of Cu by these shuttles which can lead to cuprotoxicity. We showed here that nanomolar concentrations of Cu(II)GTSM (Figure S6B), was toxic to PC12 cells, whereas the toxicity of Clioquinol and elesclomol have been previously reported[32,71]. It has equally been shown that Cu ionophores such as Elesclomol, induced the so-called cuproptosis at low nanomolar concentrations that was attributed to the Cu-induced aggregation of lipoylated mitochondrial proteins involve in Krebs cycle[72]. In addition to their lack of selectivity to Cu(II), this may partially explain why Cu ionophores, such as Clioquinol and PBT2 were unsuccessful in clinical trials against AD[33,73]. Another factor to be considered is the delivery site of these ionophores, which have tendencies to accumulate Cu in the mitochondria. Indeed, excess Cu in the mitochondria might compete with other transition metal ions (mainly Fe) and provoke mitochondrial dysfunction as well as cuproptosis[74].

Over the years, OHSCs have been used as a model to study neurodegenerative diseases, such as Parkinson[75,76] and Alzheimer[46,47] diseases, because of the similarity to *in vivo* animal models in respect to the preservation of brain connections between different cells and are hence useful in studying Aβ toxicity[77,78,79,80], oxidative stress remediation[47,81] and glial activation[82,83] in AD. In our OHSC model, we were able to induce an increased proliferation and activation of microglial cells which is believed to be associated with brain toxicity[52]. In part, this toxicity is believed to be exuberated by the extracellular redox cycling of Cu and the ROS production induced by Cu binding to ligands such as Aβ[84]. Both DapHH-αR5W4^{NBD} and HDapH-αR5W4^{NBD} seem to be capable of preventing this phenomenon. They were designed to bind extracellular Cu and import Cu into cells. However, it should be noted that the Cu importation by DapHH-αR5W4^{NBD} and HDapH-αR5W4^{NBD} were not designed to specifically target neurons. Therefore, DapHH-αR5W4^{NBD} and HDapH-αR5W4^{NBD} might also import Cu in other cells, such as microglia and astrocytes. However, it is worth mentioning that in the advent of an increase in intracellular microglial Cu levels induced by DapHH-αR5W4^{NBD} or HDapH-αR5W4^{NBD}, microglia cells do not seem to be activated (Figure 5 and S9). Therefore, if the mere presence of extracellular Cu(II), as seen in Figure 5, activates microglial (i.e. in the absence of Cu cycling), it does so directly by activating a surface receptor on microglial cells, or through ROS activation, and not through the simple increase in intracellular microglial Cu levels. In consequence, it is possible that DapHH-αR5W4^{NBD} or HDapH-αR5W4^{NBD} mitigate Cu(II) toxicity by direct binding to extracellular Cu(II) and not necessarily through the import the Cu into the cells. This remains to be further evaluated, but the former is unlikely because peptides are prone to degradation upon the 48h treatment period used here.

The mechanism by which Cu activates microglia in our case (ROS production or direct receptor activation) is yet to be determined, however, a recent work has accentuated the importance of the NLRP3 inflammasome in Cu-dependent neuro-inflammation *in vivo*. This was demonstrated by silencing Nlrp3, which lead to a decrease in Cu-dependent neuro-inflammation in toxic milk mice model[85]. The NLRP3 inflammasome is known to be activated by a plethora of chemically and structurally dissimilar stimuli, including ROS[86,87]. As a consequence, ROS produced by the cycling of Cu on a relatively weak and less stable extracellular ligand such as Aβ could lead to excess activation of microglia and consequently to neuronal damage.

In conclusion, the novel Cu(II)-selective peptide shuttles described here are capable of binding Cu(II) with high affinity and a fast enough kinetic to stop Cu(Aβ)-induced ROS production. These peptide shuttles proved to be capable of selectively retrieving extracellular Cu(II) from Aβ and importing it into a neuronal

cell model. The released Cu inside the cells was further shown to be bioavailable and nontoxic. Importantly, DapHH-αR5W4^{NBD} and HDapH-αR5W4^{NBD} shuttles, displaying distinct kinetics of Cu binding and release, were also capable of preventing OHSC slices from Cu-induced neurotoxicity, microglial proliferation and activation and therefore pose as promising drug candidates for future *in vivo* studies on AD animal models.

References

1. Dong, J. *et al.* Metal Binding and Oxidation of Amyloid-β within Isolated Senile Plaque Cores: Raman Microscopic Evidence. *Biochemistry* **42**, 2768–2773 (2003).
2. Miller, L. M. *et al.* Synchrotron-based infrared and X-ray imaging shows focalized accumulation of Cu and Zn co-localized with β-amyloid deposits in Alzheimer's disease. *J. Struct. Biol.* **155**, 30–37 (2006).
3. Reiss, A. B., Arain, H. A., Stecker, M. M., Siegart, N. M. & Kasselman, L. J. Amyloid toxicity in Alzheimer's disease. *Rev. Neurosci.* **29**, 613–627 (2018).
4. Schützmann, M. P. *et al.* Endo-lysosomal Aβ concentration and pH trigger formation of Aβ oligomers that potently induce Tau missorting. *Nat. Commun.* **12**, 4634 (2021).
5. Braak, H. & Braak, E. Neuropathological stageing of Alzheimer-related changes. *Acta Neuropathol. (Berl.)* **82**, 239–259 (1991).
6. Ma, Q.-L. *et al.* β-Amyloid Oligomers Induce Phosphorylation of Tau and Inactivation of Insulin Receptor Substrate via c-Jun N-Terminal Kinase Signaling: Suppression by Omega-3 Fatty Acids and Curcumin. *J. Neurosci.* **29**, 9078–9089 (2009).
7. Falcone, E. *et al.* Extracellular Cu2+ pools and their detection: From current knowledge to next-generation probes. *Coord. Chem. Rev.* **433**, 213727 (2021).
8. Robinson, N. J. & Winge, D. R. Copper Metallochaperones. *Annu. Rev. Biochem.* **79**, 537–562 (2010).
9. Scholefield, M. *et al.* Evidence that levels of nine essential metals in post-mortem human-Alzheimer's-brain and ex vivo rat-brain tissues are unaffected by differences in post-mortem delay, age, disease staging, and brain bank location†. *Metallomics* **12**, 952–962 (2020).
10. Schrag, M., Mueller, C., Oyoyo, U., Smith, M. A. & Kirsch, W. M. Iron, zinc and copper in the Alzheimer's disease brain: A quantitative meta-analysis. Some insight on the influence of citation bias on scientific opinion. *Prog. Neurobiol.* **94**, 296–306 (2011).
11. James, S. A. *et al.* Elevated labile Cu is associated with oxidative pathology in Alzheimer disease. *Free Radic. Biol. Med.* **52**, 298–302 (2012).
12. Rembach, A. *et al.* Decreased Copper in Alzheimer's Disease Brain Is Predominantly in the Soluble Extractable Fraction. *Int. J. Alzheimer's Dis.* **2013**, e623241 (2013).
13. Miller, L. M. *et al.* Synchrotron-based infrared and X-ray imaging shows focalized accumulation of Cu and Zn co-localized with beta-amyloid deposits in Alzheimer's disease. *J. Struct. Biol.* **155**, 30–37 (2006).
14. Schrag, M., Mueller, C., Oyoyo, U. & Kirsch, W. M. Iron, zinc and copper in the Alzheimer's disease brain: a quantitative meta-analysis. Some insight on the influence of citation bias on scientific opinion. *Prog. Neurobiol.* **94**, 296–306 (2011).
15. Cheignon, C. *et al.* Oxidative stress and the amyloid beta peptide in Alzheimer's disease. *Redox Biol.* **14**, 450–464 (2017).
16. Atrián-Blasco, E. *et al.* Cu and Zn coordination to amyloid peptides: From fascinating chemistry to debated pathological relevance. *Coord. Chem. Rev.* **375**, 38–55 (2018).
17. Falcone, E. & Hureau, C. Redox processes in Cu-binding proteins: the "in-between" states in intrinsically disordered peptides. *Chem. Soc. Rev.* **52**, 6595–6600 (2023).
18. White, A. R., Barnham, K. J. & Bush, A. I. Metal homeostasis in Alzheimer's disease. *Expert Rev. Neurother.* **6**, 711–722 (2006).
19. Bagheri, S., Squitti, R., Haertlé, T., Siotto, M. & Saboury, A. A. Role of Copper in the Onset of Alzheimer's Disease Compared to Other Metals. *Front. Aging Neurosci.* **9**, 446 (2018).
20. Atwood, C. S. *et al.* Copper Mediates Dityrosine Cross-Linking of Alzheimer's Amyloid-β. *Biochemistry* **43**, 560–568 (2004).
21. Cheignon, C., Collin, F., Sabater, L. & Hureau, C. Oxidative Damages on the Alzheimer's Related-Aβ Peptide Alters Its Ability to Assemble. *Antioxidants* **12**, 472 (2023).

22. Jenagaratnam, L. & McShane, R. Clioquinol for the treatment of Alzheimer's Disease. *Cochrane Database Syst. Rev.* (2006) doi:10.1002/14651858.CD005380.pub2.
23. Sampson, E. L., Jenagaratnam, L. & McShane, R. Metal protein attenuating compounds for the treatment of Alzheimer's dementia. *Cochrane Database Syst. Rev.* CD005380 (2014) doi:10.1002/14651858.CD005380.pub5.
24. White, A. R. *et al.* Degradation of the Alzheimer Disease Amyloid β-Peptide by Metal-dependent Up-regulation of Metalloprotease Activity*. *J. Biol. Chem.* **281**, 17670–17680 (2006).
25. Crouch, P. J. *et al.* Increasing Cu bioavailability inhibits Abeta oligomers and tau phosphorylation. *Proc. Natl. Acad. Sci. U. S. A.* **106**, 381–386 (2009).
26. Ritchie, C. W. *et al.* Metal-protein attenuation with iodochlorhydroxyquin (clioquinol) targeting Abeta amyloid deposition and toxicity in Alzheimer disease: a pilot phase 2 clinical trial. *Arch. Neurol.* **60**, 1685–1691 (2003).
27. Hegde, M. L. *et al.* Challenges Associated with Metal Chelation Therapy in Alzheimer's Disease. *J. Alzheimers Dis. JAD* **17**, 457–468 (2009).
28. Yassin, M. S., Ekblom, J., Xilinas, M., Gottfries, C. G. & Oreland, L. Changes in uptake of vitamin B(12) and trace metals in brains of mice treated with clioquinol. *J. Neurol. Sci.* **173**, 40–44 (2000).
29. Faux, N. G. *et al.* PBT2 rapidly improves cognition in Alzheimer's Disease: additional phase II analyses. *J. Alzheimers Dis. JAD* **20**, 509–516 (2010).
30. Donnelly, P. S. *et al.* Selective Intracellular Release of Copper and Zinc Ions from Bis(thiosemicarbazonato) Complexes Reduces Levels of Alzheimer Disease Amyloid-β Peptide *. *J. Biol. Chem.* **283**, 4568–4577 (2008).
31. Zhao, J. *et al.* TDMQ20, a Specific Copper Chelator, Reduces Memory Impairments in Alzheimer's Disease Mouse Models. *ACS Chem. Neurosci.* **12**, 140–149 (2021).
32. Tsvetkov, P. *et al.* Copper induces cell death by targeting lipoylated TCA cycle proteins. *Science* **375**, 1254–1261 (2022).
33. Arbiser, J. L. *et al.* Clioquinol-Zinc Chelate: A Candidate Causative Agent of Subacute Myelo-Optic Neuropathy. *Mol. Med.* **4**, 665–670 (1998).
34. Okafor, M. *et al.* Development of Cu(II)-specific peptide shuttles capable of preventing Cu–amyloid beta toxicity and importing bioavailable Cu into cells. *Chem. Sci.* **13**, 11829–11840 (2022).
35. Okafor, M. *et al.* Restoring cellular copper homeostasis in Alzheimer disease: a novel peptide shuttle is internalized by an ATP-dependent endocytosis pathway involving Rab5-and Rab14endosomes. *Front. Mol. Biosci.* **11**, (2024).
36. Lefèvre, M., Malikidogo, K. P., Esmieu, C. & Hureau, C. Sequence–Activity Relationship of ATCUN Peptides in the Context of Alzheimer's Disease. *Molecules* **27**, 7903 (2022).
37. Falcone, E., Vileno, B., Hoang, M., Raibaut, L. & Faller, P. A luminescent ATCUN peptide variant with enhanced properties for copper(II) sensing in biological media. *J. Inorg. Biochem.* **221**, 111478 (2021).
38. Stoppini, L., Buchs, P.-A. & Muller, D. A simple method for organotypic cultures of nervous tissue. *J. Neurosci. Methods* **37**, 173–182 (1991).
39. Djoko, K. Y., Donnelly, P. S. & McEwan, A. G. Inhibition of respiratory Complex I by copper(ii)-bis(thiosemicarbazonato) complexes†. *Metallomics* **6**, 2250–2259 (2014).
40. Conte-Daban, A. *et al.* Link between Affinity and Cu(II) Binding Sites to Amyloid-β Peptides Evaluated by a New Water-Soluble UV–Visible Ratiometric Dye with a Moderate Cu(II) Affinity. *Anal. Chem.* **89**, 2155–2162 (2017).
41. Kaler, S. G. ATP7A-related copper transport diseases—emerging concepts and future trends. *Nat. Rev. Neurol.* **7**, 15–29 (2011).
42. Faller, P. & Hureau, C. Reproducibility Problems of Amyloid-β Self-Assembly and How to Deal With Them. *Front. Chem.* **8**, (2021).

43. Rice, M. E., Rice, M. E. & Rice, M. E. Ascorbate regulation and its neuroprotective role in the brain. *Trends Neurosci.* **23**, 209–216 (2000).
44. Guilloreau, L., Combalbert, S., Sournia-Saquet, A., Mazarguil, H. & Faller, P. Redox chemistry of copper-amyloid-beta: the generation of hydroxyl radical in the presence of ascorbate is linked to redox-potentials and aggregation state. *Chembiochem Eur. J. Chem. Biol.* **8**, 1317–1325 (2007).
45. Chepda, T., Cadau, M., Girin, Ph., Frey, J. & Chamson, A. Monitoring of ascorbate at a constant rate in cell culture: Effect on cell growth. *Vitro Cell. Dev. Biol. - Anim.* **37**, 26–30 (2001).
46. Hoppe, J. B. *et al.* Amyloid-β neurotoxicity in organotypic culture is attenuated by melatonin: involvement of GSK-3β, tau and neuroinflammation. *J. Pineal Res.* **48**, 230–238 (2010).
47. Bruce, A. J., Malfroy, B. & Baudry, M. beta-Amyloid toxicity in organotypic hippocampal cultures: protection by EUK-8, a synthetic catalytic free radical scavenger. *Proc. Natl. Acad. Sci.* **93**, 2312–2316 (1996).
48. Hu, Z. *et al.* Subneurotoxic copper(II)-induced NF-κB-dependent microglial activation is associated with mitochondrial ROS. *Toxicol. Appl. Pharmacol.* **276**, 95–103 (2014).
49. Yan, L. *et al.* JNK and NADPH Oxidase Involved in Fluoride-Induced Oxidative Stress in BV-2 Microglia Cells. *Mediators Inflamm.* **2013**, e895975 (2013).
50. Simpson, D. S. A. & Oliver, P. L. ROS Generation in Microglia: Understanding Oxidative Stress and Inflammation in Neurodegenerative Disease. *Antioxidants* **9**, 743 (2020).
51. Ito, D. *et al.* Microglia-specific localisation of a novel calcium binding protein, Iba1. *Mol. Brain Res.* **57**, 1–9 (1998).
52. Hopperton, K. E., Mohammad, D., Trépanier, M. O., Giuliano, V. & Bazinet, R. P. Markers of microglia in post-mortem brain samples from patients with Alzheimer's disease: a systematic review. *Mol. Psychiatry* **23**, 177–198 (2018).
53. Sirangelo, I. & Iannuzzi, C. The Role of Metal Binding in the Amyotrophic Lateral Sclerosis-Related Aggregation of Copper-Zinc Superoxide Dismutase. *Mol. Basel Switz.* **22**, 1429 (2017).
54. Hayward, L. J. *et al.* Decreased metallation and activity in subsets of mutant superoxide dismutases associated with familial amyotrophic lateral sclerosis. *J. Biol. Chem.* **277**, 15923–15931 (2002).
55. Davies, K. M. *et al.* Localization of copper and copper transporters in the human brain†. *Metallomics* **5**, 43–51 (2013).
56. Genoud, S. *et al.* Subcellular compartmentalisation of copper, iron, manganese, and zinc in the Parkinson's disease brain. *Met. Integr. Biometal Sci.* **9**, 1447–1455 (2017).
57. DEXTER, D. T. *et al.* ALTERATIONS IN THE LEVELS OF IRON, FERRITIN AND OTHER TRACE METALS IN PARKINSON'S DISEASE AND OTHER NEURODEGENERATIVE DISEASES AFFECTING THE BASAL GANGLIA. *Brain* **114**, 1953–1975 (1991).
58. Popescu, B. F. G. *et al.* Mapping metals in Parkinson's and normal brain using rapid-scanning x-ray fluorescence. *Phys. Med. Biol.* **54**, 651 (2009).
59. Ayton, S. *et al.* Ceruloplasmin dysfunction and therapeutic potential for Parkinson disease. *Ann. Neurol.* **73**, 554–559 (2013).
60. Hedera, P. Wilson's disease: A master of disguise. *Parkinsonism Relat. Disord.* **59**, 140–145 (2019).
61. Nagral, A. *et al.* Wilson's Disease: Clinical Practice Guidelines of the Indian National Association for Study of the Liver, the Indian Society of Pediatric Gastroenterology, Hepatology and Nutrition, and the Movement Disorders Society of India. *J. Clin. Exp. Hepatol.* **9**, 74–98 (2019).
62. Pfeiffenberger, J. *et al.* Long-term evaluation of urinary copper excretion and non-caeruloplasmin associated copper in Wilson disease patients under medical treatment. *J. Inherit. Metab. Dis.* **42**, 371–380 (2019).
63. Kollros, P. R., Dick, R. D. & Brewer, G. J. Correction of cerebrospinal fluid copper in Menkes kinky hair disease. *Pediatr. Neurol.* **7**, 305–307 (1991).
64. Tümer, Z. & Møller, L. B. Menkes disease. *Eur. J. Hum. Genet.* **18**, 511–518 (2010).

65. Donadio, G. *et al.* A new peptide-based fluorescent probe selective for zinc(ii) and copper(ii). *J. Mater. Chem. B* **4**, 6979–6988 (2016).
66. Hu, Y., Chen, A., Kong, Z. & Sun, D. A Reversible Colorimetric and Fluorescence 'Turn-Off' Chemosensor for Detection of Cu2+ and Its Application in Living Cell Imaging. *Mol. Basel Switz.* **24**, 4283 (2019).
67. Guthrie, L. M. *et al.* Elesclomol alleviates Menkes pathology and mortality by escorting Cu to cuproenzymes in mice. *Science* **368**, 620–625 (2020).
68. Donnelly, P. S. *et al.* Selective Intracellular Release of Copper and Zinc Ions from Bis(thiosemicarbazonato) Complexes Reduces Levels of Alzheimer Disease Amyloid-β Peptide*. *J. Biol. Chem.* **283**, 4568–4577 (2008).
69. Mena, S. *et al.* Drastic Effect of the Peptide Sequence on the Copper-Binding Properties of Tripeptides and the Electrochemical Behaviour of Their Copper(II) Complexes. *Chem. – Eur. J.* **24**, 5153–5162 (2018).
70. Gonzalez, P. *et al.* Cu(II) Binding to the Peptide Ala-His-His, a Chimera of the Canonical Cu(II)-Binding Motifs Xxx-His and Xxx-Zzz-His. *Inorg. Chem.* **56**, 14870–14879 (2017).
71. Benvenisti-Zarom, L., Chen, J. & Regan, R. F. The oxidative neurotoxicity of clioquinol. *Neuropharmacology* **49**, 687–694 (2005).
72. Tsvetkov, P. *et al.* Copper induces cell death by targeting lipoylated TCA cycle proteins. *Science* **375**, 1254–1261 (2022).
73. Quinn, J. F., Crane, S., Harris, C. & Wadsworth, T. L. Copper in Alzheimer's disease: too much or too little? *Expert Rev. Neurother.* **9**, 631–637 (2009).
74. Vallières, C., Holland, S. L. & Avery, S. V. Mitochondrial Ferredoxin Determines Vulnerability of Cells to Copper Excess. *Cell Chem. Biol.* **24**, 1228-1237.e3 (2017).
75. Moudio, S. *et al.* Exposure of α-Synuclein Aggregates to Organotypic Slice Cultures Recapitulates Key Molecular Features of Parkinson's Disease. *Front. Neurol.* **13**, (2022).
76. Stahl, K., Skare, Ø. & Torp, R. Organotypic Cultures as a Model of Parkinson´s Disease. A Twist to an Old Model. *Sci. World J.* **9**, 811–821 (NaN/NaN/NaN).
77. Feller, A. E. Technic and Application of Roller Tube Cultures. in *Handbuch der Virusforschung: II. Ergänzungsband* (eds. Doerr, R. et al.) 1–10 (Springer, Vienna, 1950). doi:10.1007/978-3-7091-5688-9_1.
78. Wray, S. Organotypic Slice Explant Roller-Tube Cultures. in *Practical Cell Culture Techniques* (eds. Boulton, A. A., Baker, G. B. & Walz, W.) 201–239 (Humana Press, Totowa, NJ, 1992). doi:10.1385/0-89603-214-0:201.
79. Suh, E. C., Jung, Y. J., Kim, Y. A., Park, E. M. & Lee, K. E. Aβ25–35 induces presynaptic changes in organotypic hippocampal slice cultures. *NeuroToxicology* **29**, 691–699 (2008).
80. Frozza, R. L. *et al.* A Comparative Study of β-Amyloid Peptides Aβ1-42 and Aβ25-35 Toxicity in Organotypic Hippocampal Slice Cultures. *Neurochem. Res.* **34**, 295–303 (2009).
81. Clapp-Lilly, K. L. *et al.* Melatonin acts as antioxidant and pro-oxidant in an organotypic slice culture model of Alzheimer's disease. *NeuroReport* **12**, 1277 (2001).
82. Richter, M. *et al.* The neuroprotective role of microglial cells against amyloid beta-mediated toxicity in organotypic hippocampal slice cultures. *Brain Pathol.* **30**, 589–602 (2020).
83. Novotny, R. *et al.* Conversion of Synthetic Aβ to In Vivo Active Seeds and Amyloid Plaque Formation in a Hippocampal Slice Culture Model. *J. Neurosci.* **36**, 5084–5093 (2016).
84. Patel, R. & Aschner, M. Commonalities between Copper Neurotoxicity and Alzheimer's Disease. *Toxics* **9**, 4 (2021).
85. Dong, J. *et al.* Inhibiting NLRP3 inflammasome activation prevents copper-induced neuropathology in a murine model of Wilson's disease. *Cell Death Dis.* **12**, 1–12 (2021).

86. Lamkanfi, M. & Kanneganti, T.-D. Nlrp3: An immune sensor of cellular stress and infection. *Int. J. Biochem. Cell Biol.* **42**, 792–795 (2010).
87. Kelley, N., Jeltema, D., Duan, Y. & He, Y. The NLRP3 Inflammasome: An Overview of Mechanisms of Activation and Regulation. *Int. J. Mol. Sci.* **20**, 3328 (2019).